

Physics Informed Neural Networks for Dynamic Load Reconstruction for Plant Piping

Subrata Saha

Department of Mechanical Engineering, Techno India University, Sector V, Salt Lake, Kolkata, West Bengal, India

Abstract

This study aims to offer a method for calculating the dynamic loads on a vibrating pipework in a process plant based on the Theory of Inverse Problems (IP) and physics-informed neural networks (PINN). Vibrating pipes present a significant risk of fatigue failure, which can potentially cause catastrophic damage. However, the lack of quantitative information on applied loads precludes the conventional design of the system. Mathematically, the governing partial differential equation (PDE) is ill-posed. In this scenario, a data-driven strategy based on neural networks was studied in an inverse theoretical framework was studied. Deep Neural Networks (DNNs) were used to model the forcing function, and the PDE was solved in the time domain for the displacement response. The target data were the displacement readings of the in-situ vibration. This problem is reduced to an optimization problem that minimizes the errors. Two cases, one with single loading and the other with dual loading, were presented to validate the theory. These results clearly demonstrate the effectiveness of the proposed method. The widespread use of artificial intelligence (AI) and machine learning (ML) in multidisciplinary engineering domains is the main motivating factor. This study is significant from the perspective of monitoring industrial equipment conditions.

Keywords Physics Informed Neural Networks (PINN); Artificial Intelligence (AI); Inverse Problem (IP); Piping Vibration; Force Reconstruction; Vibration Frequency

1. Introduction

Vibration failures of piping are a serious problem and a safety hazard for plant operations [1-6]. Historically, piping vibration failures have been reported as a major cause of plant outages, explosions, and fire incidents over a period of 30 years [2]. An operating piping carrying a service fluid experiences various mechanical loads throughout its life cycle. The moving fluid induces a vibratory motion at various points on the piping system. Excessive vibration can lead to fatigue failure if the fluctuating stresses exceed the endurance limit of the material, which is a potential risk in terms of safety and asset integrity management [4]. Hence, engineering designs should provide safeguards for piping systems against such failures. The design procedure calculates the induced dynamic stresses and keeps them within allowable limits by suitably modifying the design parameters.

The vibration is flow-induced, and forces are induced on the piping through the pressure acting on the inside walls of the pipes. However, owing to the complexity of this phenomenon, no closed-form analytical expressions were available for the forcing function. This precludes the determination of stresses by using the conventional method for solving the PDE. The current practice in industry is to use a vibration

screening method [5-9]. In this method, in situ vibration measurements are taken on the vibrating pipes, and the readings are compared against some permissible limiting values as per the severity charts [7-9]. Instruments, such as portable vibrometers, are normally used for data acquisition [10].

Vibration levels were classified as either acceptable (safe) or dangerous (unsafe). For high vibration levels, reduction is sought by quick fix methods such as support additions. This is a hit and trial approach, and in many cases, has serious implementation problems. Thus, there is a real need to develop analytical methods to assess the actual vibration levels to provide an effective engineering solution to this problem.

If the governing PDE is well defined along with the boundary conditions, the problem is termed as well-posed [11-14] and conventional methods can be employed for the solution. This type of problem, which admits a direct solution, is also known as the forward problem. However, in our case, the forcing function is unknown, and thus the forward problem is ill-posed [11-14]. For this class of problems, it is imperative to invoke the theory of Inverse Problems [11] to obtain a solution. Typically, the problem is expressed in the form of an integral equation [11], and the observations that form the data are normally measurements of the field variables, either at the interior points or boundary. Mathematically, the existence and uniqueness of a solution and its reconstruction constitute the primary areas of study.

2. Literature Survey

The paper by Moussa et. al. [15] was one of the earliest studies to present an analytical approach. Their study estimated dynamic stresses from field measurements of industrial piping. Although their objective was to calculate the stresses without reconstructing the unknown forces, they provided significant insight into the application of the Inverse Theory. Based on their method, an FEA [16] model of the piping was developed, and the displacement time histories (which simulate the observations) were imposed at the observation points. The dynamic stresses resulting from imposed displacements were evaluated. The major difference compared with our case is that, in their study, the locations of the forces were unknown. Although this poses additional complications, an appropriate mathematical analysis has not been conducted. Their approach was mainly heuristic but simple to adopt.

For hyperbolic systems, Bruckner et al. studied the determination of point sources. al. [17]. This is an important problem for the development of earthquake models. Yamamoto [18] studied the problem of determining the point forces for vibrating plates and beams was studied by Yamamoto [18]). Mathematical proofs of uniqueness, existence, and stability were presented in this study. Nicaise et. al. [19] studied the problem of determining the point loads on vibrating beams. This finding was closely related to the results of the present study. However, the major difference is the nature of the applied loads, for which the time-varying function is known a priori and is unknown in our case. The location of the forces was unknown in [16], whereas in our study, the locations of the forces were known a priori. Based on Inverse Theory, it has been shown in [18,19] that with some interior or boundary observations, it is possible to estimate point loads. Nicaise et. al. [19] presented a reconstruction strategy for estimating point loads in addition to the proofs of the existence and uniqueness of the solution. In the aforementioned studies, the displacements for the interior measurements or slopes were considered as the boundary measurements for the vibrating beams. The time-varying functions also exhibit specified degrees of smoothness and continuity. Saha [5] has applied a reconstruction strategy to solve real-life problems.

Saha's study [1] was likely the first to explore using PINN for load reconstruction in plant piping, though it focused on a single point load with limited mathematical detail. The present investigation expands upon this foundation, offering a more comprehensive theoretical framework and in-depth analysis of findings.

It addresses both single and dual point loads, and also calculates dynamic stresses on the piping to assess structural integrity, creating a more thorough examination.

With the advent of high-power computing resources and advancements in machine learning techniques, data-driven approaches using PINNs [20,21] are gaining popularity. The use of PINNs to solve PDE's is relatively new. The mathematical basis of the ability of a DNN to solve PDE's can be attributed to the uniform approximation theorem proposed by Hornik et al. [22]. Based on this theorem, the DNN model can satisfy the PDE as a solution to the constrained optimization problem. In this respect, PINN's are more efficient at solving inverse problems than direct problems; for the latter, a relatively large number of parameters must be optimized. The convergence properties of PINNs for nonlinear elliptic and parabolic PDE have been studied by Shin et al. [23]. This provides a sound mathematical justification for the method, which has hitherto been empirically successful. Lu et. al. [24] studied the developed learning NN models called DeepONets based on universal approximation theory for non-linear operators.

The motivation for the present work has been drawn from growing research work in diverse areas, such as delineated above. A major factor conducive to research is the proliferation of open-source software for AI/ML in the public domain. Several software packages are available for scientific computing, providing researchers with a wide range of choices. Last but not the least, the easy availability of powerful hardware is instrumental for the upsurge in the research work in this field.

The remainder of this paper is organized as follows. Section 3 and its subsections delve into the mathematical details of this problem. The equilibrium equation for the beam vibration or the PDE of the forward problem is as follows: The mathematical proofs of the existence and uniqueness of the forward problem are presented in Appendix A. In subsection 3.1, the formulation of the Inverse Problem (IP) is discussed. The proof of existence and uniqueness of this IP is presented in Appendix B. The DNN model for the IP and loss functions is described in section 4. As part of the validation of the proposed method, numerical experiments are presented in section 5, and the results are discussed in section 6. Finally, a summary and concluding remarks are presented in Section 7.

3 Mathematical Formulation

3.1 Nomenclature

Notation	Description
L	Length of the beam
Ω	Interval $(0, L)$
T	End Time
M	Number of observation points
P	Number of force application points
$C(X)$	Space of continuous functions in domain (X)
$C^k(X)$	Space of functions in domain (X) whose k th derivative $\in C(X)$
$L^2(\Omega)$	Space of square integrable functions, defined as: $\{f(x): \int_{\Omega} f ^2 dx < \infty\}$
$\ f\ _{0,\Omega}$	Norm of $L^2(\Omega)$ function defined as: $\{\int_{\Omega} f ^2 dx\}^{1/2}$
$D^k(w)$	derivative of k th order is defined as $\frac{\partial^k w}{\partial x^k}$
$H^m(\Omega)$	Sobolev Space of order m , defined as: $\{f : \frac{\partial^k f}{\partial x^k} \in L^2(\Omega); k = 0 \text{ to } m\}$
$\ f\ _{m,\Omega}$	Norm of $f(x)$ in $H^m(\Omega)$, defined as: $\{\ f\ _{0,\Omega}^2 + \sum_{k=1}^m \int_{\Omega} \frac{\partial^k f}{\partial x^k} ^2 dx\}^{1/2}$

$C([0, T], X)$	Map from $[0, T]$ to X , defined as: $\{w: [0, T] \rightarrow X; w \in C[0, T]; w(t, x) \in X \text{ for any fixed } t\}$
$C^n([0, T], X)$	Map from $[0, T]$ to X Defined as: $\{w: ([0, T] \rightarrow X); \frac{\partial^n w}{\partial t^n} \in C([0, T]); w(t, x) \in X \text{ for any fixed } t\}$
m	Mass per unit length of the pipe/beam
c	Damping Coefficient
EI	Bending Rigidity
$\delta(x - x_k)$	Dirac Delta Function
$f_k(t)$	Forcing function at location
u, \dot{u}, \ddot{u}	Displacement, Velocity and Acceleration (resp.) at an interior point
\bar{u}	Observation data for Displacement
ω_n	Circular Natural Frequency for the n^{th} mode.
ζ_n	Critical modal damping ratio for the n^{th} mode.
ζ	Critical damping ratio
$\phi_n(x)$	Mass normalized eigen-vector for the n^{th} mode.
$q_n^k(t)$	Modal displacement response for forcing function f_k
$\dot{q}_n^k(t)$	Modal velocity response for forcing function f_k

3.2 Equilibrium Equation of the system

Figure 1 depicts the physical model of a pipe that is simply supported at ends A and B . The length of span AB is L , and the concentrated forces act at P points x_1, x_2, \dots, x_p . The equilibrium equation for the vibration of a uniform beam is given by Equation (1) [1]. The mass per unit length is m , the damping coefficient c and the flexural rigidity EI . The displacement variable is denoted by u , where a dot refers to the time differentiation and D^n is the n th-order partial derivative with respect to the space variable x . The boundary conditions correspond to those of a simply supported beam and the initial conditions correspond to those of a beam initially at rest.

The forcing function $F(x, t)$ is expressed as a weighted delta function in space as shown in Equation (2). The weighing function is $f_k(t)$ which is time varying and is applied at point x_k . Mathematically, the function $F(x, t)$ can be understood in terms of distribution [26].

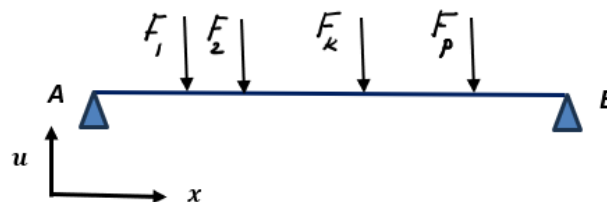


Fig.1 Simply supported pipe loaded with concentrated forces

$$m\ddot{u}(t, x) + c\dot{u}(t, x) + EID^4u(t, x) = F(x, t) \quad (\text{for } x \in \Omega) \dots\dots\dots (1)$$

$$F(x, t) = \sum_{i=k}^K \delta(x - x_k) f_k(t) \dots\dots\dots (2)$$

Boundary Conditions (B. C's):

$$u(t, 0) = 0 \quad u(t, L) = 0 \dots\dots\dots (3)$$

$$EID^2 u(t, 0) = 0 \quad EID^2 u(t, L) = 0 \dots\dots\dots(4)$$

Initial Conditions (I,C's):

$$u(0, x) = 0 \quad \dot{u}(0, x) = 0 \dots\dots\dots(5)$$

3.3 Forward Problem

For Equation (1) to be well posed, it is necessary that the forcing function $F(x, t)$, the BC's (Equations (3) and (4)), IC's (Equation (5)), and the material and geometric properties be completely defined. In this case, it is possible to prove the existence of a solution (in the classical sense) and its uniqueness. We present the proof in section 3.4 under certain assumptions on the smoothness properties of the forcing function. This approach follows the method adopted by Nicaise et al. al. [19]. The essential components are the eigen expansion or mode superposition principle [25] for vibrating systems, and the convergence of functions expressed as a series. It has been shown that, for some suitable function spaces, the forward problem has a unique solution.

We now describe the method for finding a solution to the forward problem based on the mode-superposition principle. Let u^k denote the displacement response of forcing function f_k . Then, from Equation (1), we obtain the equilibrium equation:

$$m\ddot{u}^k(t, x) + c\dot{u}^k(t, x) + EID^4 u^k(t, x) = \delta(x - x_k) f_k(t) . \dots\dots\dots (6)$$

B. C and I. C are identical to (3) and (4), with u^k replacing u .

In *RHS* of Equation (6), $\delta(x - x_k)$ is the Dirac Delta Function [37].

By applying the mode-superposition principle, the displacement solution of Equation (6) can be expressed in terms of modal components as follows:

$$u^k(t, x) = \sum_{n=1}^{\infty} \phi_n(x) q_n^k(t) \dots\dots\dots(7)$$

Here, the term ϕ_n denotes the mass-normalized eigenvector and $q_n^k(t)$ denotes the modal displacement for the n th. should be noted that the BC's are identically satisfied by the eigenvectors. The total displacement $u(x, t)$ is then obtained as the sum of the displacements resulting from the individual loads.

$$u(t, x) = \sum_{k=1}^P u^k(t, x) \dots\dots\dots(8)$$

To obtain the modal equations, we adopted the standard procedure of multiplying Equation (7) by ϕ_n and integrating over the domain (Ω). Using the orthogonal properties of the eigenvectors [36], we obtained modal equations in an uncoupled form.

$$\ddot{q}_n^k(t) + 2\omega_n \zeta_n \dot{q}_n^k(t) + \omega_n^2 q_n^k(t) = \phi_n(x_k) f_k(t) \dots\dots\dots(9)$$

(where ω_n denotes the undamped natural frequency and ζ_n the critical damping ratio for the n^{th} mode)

From the IC's (6), the modal components obtained are

$$q_n^k(0) = 0 \qquad \dot{q}_n^k(0) = 0 \qquad \dots\dots\dots(10)$$

The closed-form solution of Equations (8)–(10) can be obtained from Duhamel’s integral [7], as follows:

$$q_n^k(t) = \left(\frac{1}{\omega_{dn}}\right) \int_0^t F_n^k(\tau) e^{-\zeta_n \omega_n(t-\tau)} \sin(\omega_{dn}(t-\tau)) d\tau \qquad \dots\dots\dots(11)$$

Here the following notations have been used

$$F_n^k(t) = \Phi_n(x_k) f_k(t) \qquad \dots\dots\dots(12)$$

The damped natural frequency $\omega_{dn} = \omega_n \sqrt{1 - \zeta_n^2}$

Using Equations (7-11) we obtain an expression for the displacement:

$$u(t, x) = \sum_{k=1}^P \sum_{n=1}^{\infty} \phi_n(x) \left(\frac{1}{\omega_{dn}}\right) \int_0^t F_n^k(\tau) e^{-\zeta_n \omega_n(t-\tau)} \sin(\omega_{dn}(t-\tau)) d\tau \qquad \dots\dots\dots(13)$$

For a simply- supported beam, the undamped natural frequencies are given as

$$\omega_n = \left(\frac{n\pi}{L}\right)^2 * \sqrt{\frac{EI}{m}} \qquad \dots\dots\dots(14)$$

The mass normalized eigen-vectors are $\phi_n(x) = \sqrt{\frac{2}{mL}} \sin\left(\frac{n\pi x}{L}\right)$ $\dots\dots\dots(15)$

From the IC’s (6), the modal components obtained are

$$q_n^k(0) = 0 \qquad \dot{q}_n^k(0) = 0 \qquad \dots\dots\dots(10)$$

The closed-form solution of Equations (8)–(10) can be obtained from Duhamel’s integral [36] as follows:

$$q_n^k(t) = \left(\frac{1}{\omega_{dn}}\right) \int_0^t F_n^k(\tau) e^{-\zeta_n \omega_n(t-\tau)} \sin(\omega_{dn}(t-\tau)) d\tau \qquad \dots\dots\dots(11)$$

Here the following notations have been used

$$F_n^k(t) = \Phi_n(x_k) f_k(t) \qquad \dots\dots\dots(12)$$

The damped natural frequency $\omega_{dn} = \omega_n \sqrt{1 - \zeta_n^2}$

Using Equations (7-11) we obtain an expression for the displacement

$$u(t, x) = \sum_{k=1}^P \sum_{n=1}^{\infty} \phi_n(x) \left(\frac{1}{\omega_{dn}}\right) \int_0^t F_n^k(\tau) e^{-\zeta_n \omega_n(t-\tau)} \sin(\omega_{dn}(t-\tau)) d\tau$$

.....(13)

For a simply- supported beam, the undamped natural frequencies are given as

$$\omega_n = \left(\frac{n\pi}{L}\right)^2 * \sqrt{\frac{EI}{m}}$$

.....(14)

The mass normalized eigen-vectors are $\phi_n(x) = \sqrt{\frac{2}{mL}} \sin\left(\frac{n\pi x}{L}\right)$ (15)

3.4 Existence and Uniqueness of the Forward Problem

Details are given in Appendix A.

3.5 Inverse Problem

Equation (13) can be transformed into an integral equation for the Inverse Problem (IP) in the following manner.

$$\sum_{k=1}^P \sum_{n=1}^{\infty} \phi_n(x) \left(\frac{1}{\omega_{dn}}\right) \int_0^t F_n^k(\tau) e^{-\zeta_n \omega_n(t-\tau)} \sin(\omega_{dn}(t-\tau)) d\tau = \bar{u}(t, x)$$

.....(16)

The *RHS* is to be construed as the measurements or observations.

The solution of Equation (16) is the forcing function, which is composed of *P* different time functions at *P* loading points. The *RHS* constitutes the time history of displacement observations. It is implied that observations, which are in situ vibration measurements, satisfy the BC's (Equations (3,4)) and IC's (Equation (5)).

Conventionally, the mathematical aspects investigated are the existence and uniqueness of the solution, stability, and the reconstruction strategy of the solution [18,19], which is the forcing function in our case. This study of existence deals with the question of whether a solution to Equation (16) exists. Even if a solution exists, the question remains as to whether it is unique. The study of stability delves into the question of whether the forcing function is bound by observational data under some norms. This ascertains whether there is a continuous dependence of the solution on data. The third aspect of this study is the determination of the observability estimates. This reconstruction study aimed to develop a theoretical procedure for determining the forcing function.

Yamamoto et al. [18], Nicaise et al. [19] studied the problem of determining the point-wise load for vibrating beams based on the observation of the slopes at the boundaries and displacements at the interior points. Their study mathematically addresses these topics. In these studies, a single-time form of the forcing function was assumed to be known. This time form acts at different points on the piping, differing only in scale, whose factors are expressed as the weights of the Dirac delta function at the application points. The locations of the forces and weights are unknown, and are obtained as a solution to the IP. The forcing function was assumed to be nonzero at the initial time $t = 0$. This condition is necessary to obtain a solution for certain integral equations [19]. An undamped system is considered in these studies. By contrast, our case assumes that the locations of the forcing functions are known a priori, but the time form of the forcing functions is unknown. In addition, viscous damping was considered, which is more realistic.

For our problem, the proof of existence and uniqueness of the inverse problem are provided in Appendix B. Neural networks have been used as a reconstruction strategy to model the forcing function, which is a novel approach to this class of problems. Subsequently, the problem was formulated as a multivariable optimization. The objective function is the loss function calculated from the difference between the measured and calculated displacements. The mean-square norm of the loss function is minimized when the PDE (Equation (1)) is satisfied as a constraint.

3.6 Existence and Uniqueness of Inverse Problem

Details are given in Appendix B.

4 PINN – Neural Network

A schematic of the PINN Model [1] is shown in Fig. 2. The input layer consists of a single node that uses the time variable as input. The output layer consists of P nodes, each of which corresponds to the value of the forcing function, f_i at point x_i .

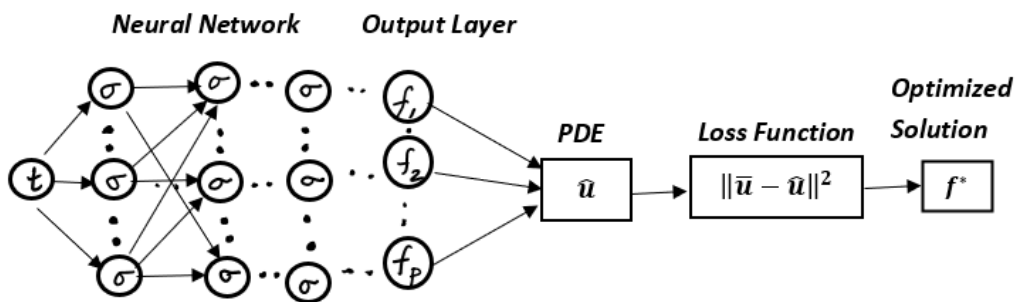


Fig. 2: Schematic of DNN Model

The Neural Network model is defined as follows:

Input Layer: $\mathcal{N}^0(t) = t \in \mathbb{R}$

Hidden Layers: $\mathcal{N}(t) = \sigma(W^l \mathcal{N}^{l-1} + b^l) \in \mathbb{R}^l$ for $1 \leq l \leq LL - 1$

Output Layer: $\mathcal{N}^{LL}(t) = \sigma(W^L \mathcal{N}^{L-1} + b^L) \in \mathbb{R}^P$

The model represents a single-input multiple-output system. The output is a vector consisting of the elements of the forcing functions at P points, where LL denotes the number of layers, W^l is the weight, b^l is the bias for layer l and σ is the activation function.

$$H_k f_k(t) = \mathcal{N}_k^{LL}(t) \quad \text{for} \quad 1 \leq k \leq P \quad \dots\dots\dots(17)$$

From Eq. 10, the modal displacement can be expressed as

$$q_n^k(t) = G_n^k(\mathcal{N}_k^L(t)) \quad \dots\dots\dots(18)$$

The approximation for the displacement function is given as

$$\hat{u}(x, t) = \sum_{k=1}^P \sum_{n=1}^N \phi_n(x) \mathcal{N}_k^L(t) \quad \dots\dots\dots(19)$$

4.1 Loss Functional

The loss function is defined as the magnitude of the residual, which is the square of the magnitude of the difference between the true displacement and output from the model. The residual R_{ki} is defined as the difference between the k th observation $\bar{u}(x_k, t_i)$ and the model output at time t_i .

$$R_{ki} = |\bar{u}(x_k, t_i) - u(x_k, t_i)| \dots\dots\dots(20)$$

The loss functional is given as

$$Loss = (0.5) * (\frac{1}{MP}) \sum_{i=1}^M \sum_{k=1}^P R_{ki}^2 \dots\dots\dots(21)$$

(Where M denotes the number of observation points.)

$$Loss(\Theta) = 0.5(\frac{1}{NT}) \sum_{i=1}^{NT} \sum_{j=1}^M |\bar{u}(x_j, t_i) - \hat{u}(x_j, t_i)|^2 \dots\dots\dots(22)$$

(Where Θ represents the vector of training parameters)

Problem is to minimize the loss function with respect to the optimization parameters.

$$\Theta^* = \text{Arg. Minimum } loss(\Theta) \dots\dots\dots(23)$$

5. Numerical Simulation

The problem of determining forces was studied in two cases. Table 1 lists the geometric and material properties of the piping system. The first case (Case 1) involved the application of a single concentrated force. In this case, two subcases (1.1 and 1.2) have been studied. These corresponded to the locations of the observation points for a fixed applied force [Table 2].

In the second case (Case 2), the loading consisted of two concentrated forces. [vide Table 3]. As in Case 1, there are two subcases corresponding to different locations of the observation points. For subcase 2.1, the locations of the observation point and the force (**Force-2**) coincide. This was performed to investigate any possible impact on the results for this special case in Case 1.

Table 1: Physical properties of the system

L (m)	m (kg/m)	EI (N-m ²)	c (N-s/m)
6	49	6860655	100

Case 1:

Table 2: Single Loading on the pipe span

<i>Sub-case</i>	<i>Force Location (m)</i>	<i>Obs. Point P₁ (m)</i>
1.1	3	3
1.2	3	2.4

Case 2:

<i>Sub-case</i>	<i>Location of Force-1 (m)</i>	<i>of Location of Force-2 (m)</i>	<i>Obs. Pt. P₁ (m)</i>	<i>Obs. Pt. P₂ (m)</i>
2.1	3	2.75	3	2.4

2.2	3	2.75	1.5	4.0
-----	---	------	-----	-----

Table 3: Dual loading in a pipe span

Our methodology consists of solving forward problem (1) with forcing functions that are assumed to be known a priori. The displacements obtained from the forward problem were treated as synthetic displacements, representing the observations that formed the target data for the inverse problem. The model was optimized to minimize the loss function (22). The output from the trained model is the force–time history.

The output forces were compared to the assumed forces to estimate the accuracy of the results. To ensure completeness, the displacement responses of the forces from the model output were calculated to ensure completeness. This was compared with the forward problem solution to assess the closeness of the match.

Random noise was added to the displacement data to simulate the real-life scenarios. The maximum variation is maintained at a displacement amplitude of 5 %. Three modes (N) were considered, which is adequate because the effect of the higher modes becomes less significant. The time interval (in seconds) is $I = [0, 0.5]$, that is, $T = 0.5$ secs, with the number of time steps $NT = 1024$.

6 Results and Discussion

In this section, the results of numerical simulations for Cases 1 and 2 are discussed.

Case 1:

The model parameters are shown below.

Number of Input layer = 5

Number of neurons per layer = 130

Number of output layer = 1

Number of trainable variables = 68511

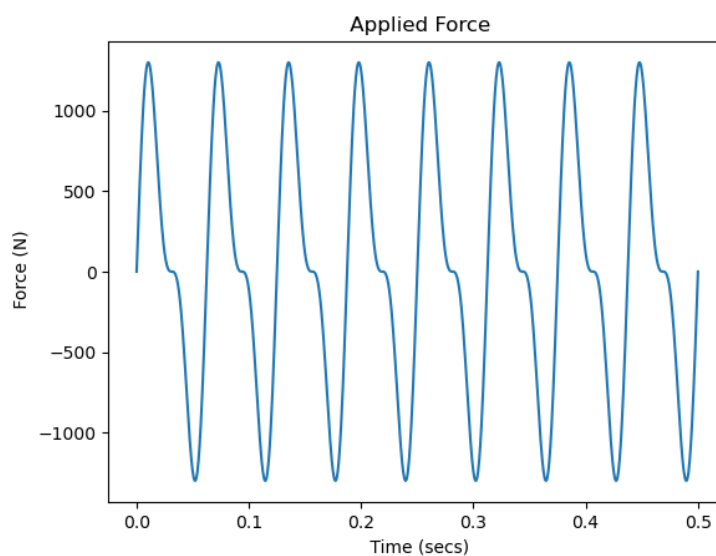


Fig. 3 Force Time History of single loading – Case:1

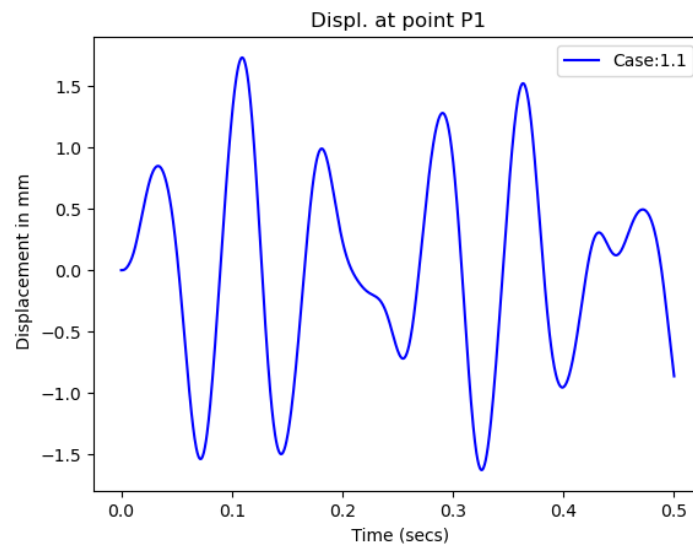


Fig. 4 Displacement Plot (Forward Problem) at point P_1

Figure 3 shows the force–time history plot for single-point loading. This is a combination of two frequency components, as shown in the plot. In Case1.1, the observation point coincided with the loading point. The displacement response for the forward problem is illustrated in Fig.4. The displacement time history forms the target response at observation point P_1 .

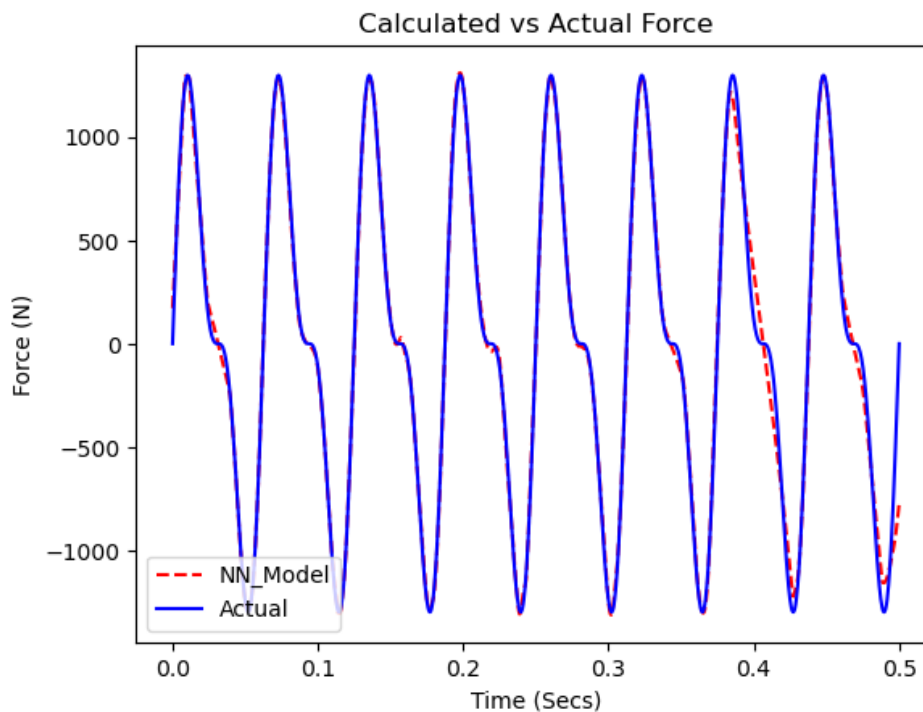


Fig. 5 Model output vs actual force – Case:1.1

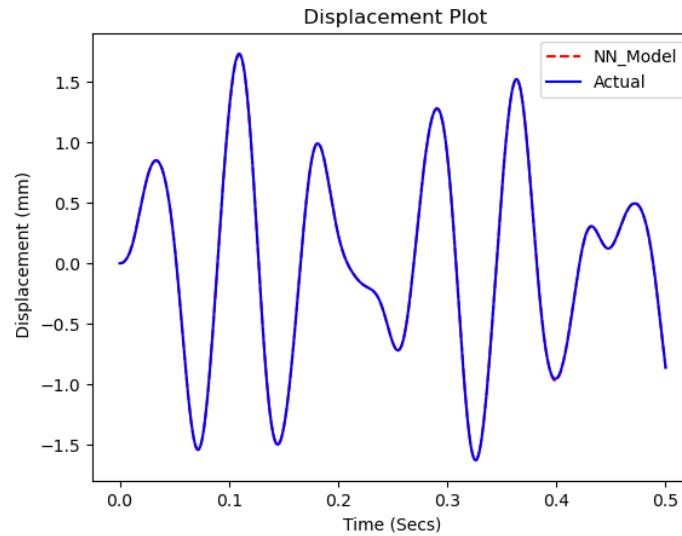


Fig. 6 Displacements - Forward vs Inverse Problem – Case:1.1

A plot of the calculated model output versus the applied force-time history is shown in Fig. 5. A close match is observed. The loss is of the order of $1.0E-04$, which is quite low and thus indicates the stability of the method. Thus, we can conclude that the NN model can successfully control errors in noisy data. As a completeness check, the displacement response was calculated for forces from the model output. The displacement-time plots of point P1 (observation vs. response calculated from the model output) are shown in Fig.6. Again, we observed that this deviation was extremely low. This demonstrated the effectiveness of the PINN method.

In Case 1.2, the loading and observation points were different. However, the trend of the results greatly resembled that of case 1.1. Thus, for brevity, the results for Case 1.2 were not obtained herein. However, these simulations clearly indicate that the relative locations of the observations and loading points did not affect the accuracy of the results. This guarantees the reconstruction of the forces with high reliability.

Case 2:

The model parameters were kept the same as those of Case 1, with only the difference in the number of output layers being two, which corresponds to the dual loading points. Figure 7 shows the applied loading. The forward problem is solved for the displacements at observation points P_1 and P_2 . Random noise, as in Case 1, was added to the calculated displacements to form the target displacement functions [Figure 8].

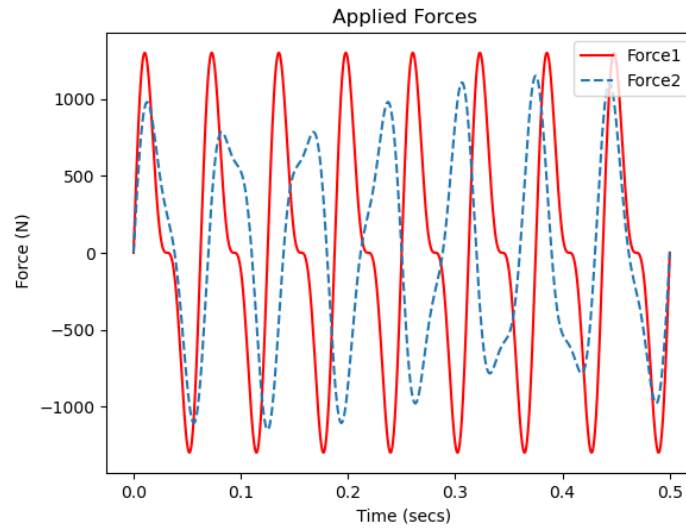


Fig. 7 Force Time History at dual loading points – Case: 2

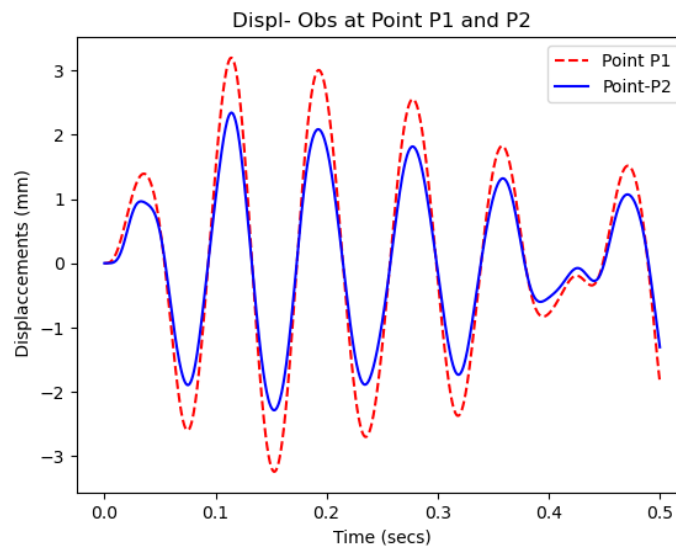


Fig. 8 Displacements at Observation Points- Case: 2.1

The plots of the output forces from the model versus the actual loadings are shown in Figs 9 and 10. The loss is on the order of $1.0E-04$, and we also obtain stability for the dual-loading case. As in Case 1, a close match is observed between the forces. The displacements of the forces from the model outputs are then calculated. Plots of the displacements at the observation points are shown in Figs. 11 and 12. This deviation is quite low and this demonstrated the effectiveness of the NN model for multiple loadings. For Case 2.2, the results were similar to those for Case 2.1; hence, they have not been reported.

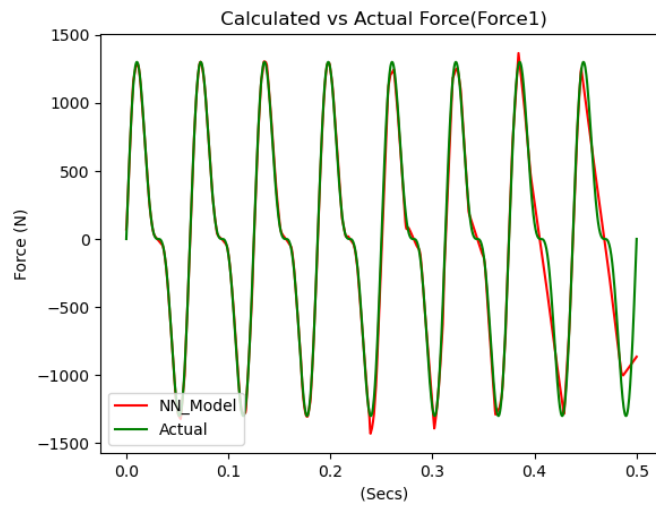


Fig. 9: Model output vs actual force (Force1)– Case:2.1

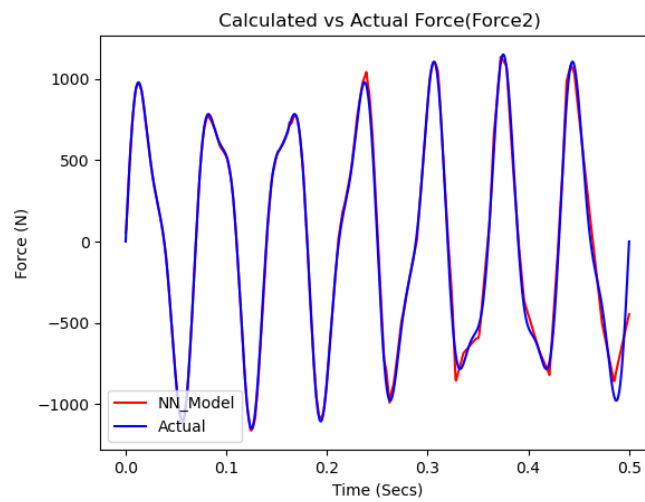


Fig. 10: Model output vs actual force (Force2)– Case:2.1

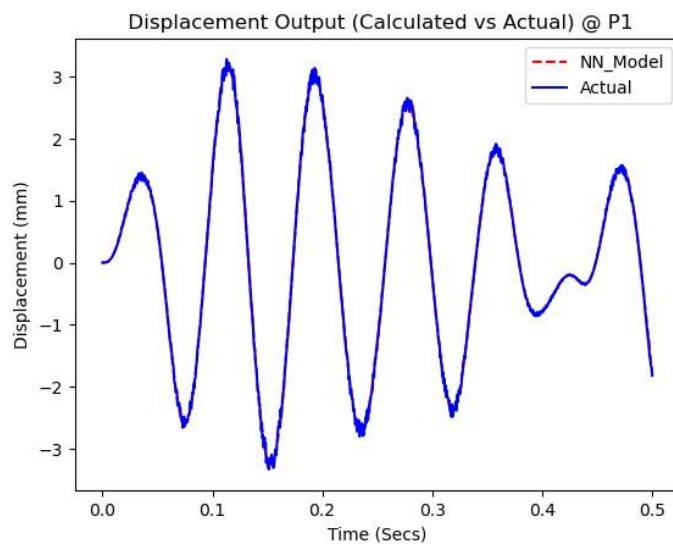


Fig. 12: Displacement: Model Output vs Input @ P_2 - Case:2.1

6.1 Initialization of the training parameters.

The performance of an NN model depends largely on the initialization of the training parameters, the selection of which is a major challenge. The default values result in an extremely slow convergence; in some cases, convergence is not guaranteed, even for a large number of epochs. This is an area of concern for the ML process, and recently, there has been some work in this direction by Wang et. al. [27], and Jacot et. al. [28]. The authors studied the initialization process in a functional analysis setting and developed a kernel function called the Neural Tangent Kernel (NTK). This is significant for analyzing training dynamics using kernel functions or Gaussian processes.

This convergence problem was also observed in this case. However, to make the appropriate choice, it is essential to understand the physics of the problem. Our approach is heuristic, in which the initialized parameters are finalized by scaling after several trials. However, the physics of the relationship between the input and output form the theoretical basis of the initialization process.

By inspecting Equation. (6), we can assume a scale factor EI (bending rigidity) between the displacement and force terms. Thus, the displacement time history was scaled up by EI to estimate the initial forcing function, which was considered the target function for the model fit by regression. The initial parameters are obtained by fitting the model to the force function. Further fine-tuning was performed on the scale factor to improve performance.

6.2 Stress Evaluation based on the Model Output

The mechanical integrity of the system is determined by the vibration-stress levels. The dynamic stresses must be maintained below the allowable stress based on the endurance limit of the material. To check the stresses, the force–time history obtained from the NN model was applied to the piping system, and the results were observed. Figure 13 shows the stress plot of the 3D-FEA model for Case 1.

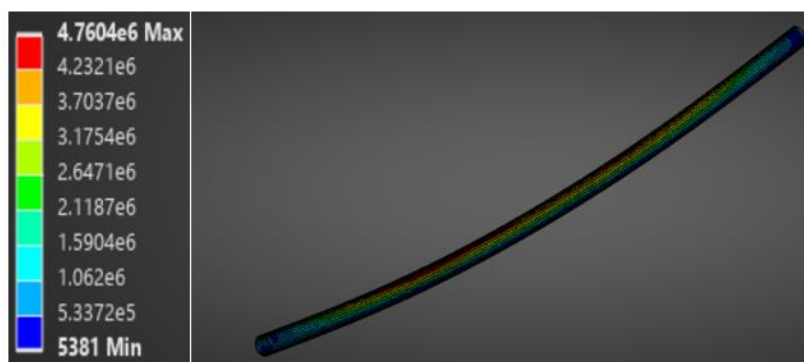


Fig. 13: Stress Contour Plot for 3D FEA model (Case-1)

A maximum stress of magnitude 4.7 MPa was reported, which was much lower than the allowable stress of 84 MPa for carbon steel. Thus, piping is considered safe under vibratory loads.

7 Conclusion

A novel method for load reconstruction was presented. The theoretical basis for this is the theory of the inverse problem theory. However, the PINN method was adopted in the numerical solution strategy. The key factors behind this motivation have been the rapid development of AI/ML techniques in engineering applications, the availability of open-source software, and advanced computing resources. The success of

this method was demonstrated through numerical experiments, as described in this study. The most challenging step is the initialization of the training parameters. This critically governs the convergence rate and the solution time. A heuristic approach is adopted in this case. It is evident that considerable research is required to understand the effect of activation functions on the convergence rate. This is a potential topic for further study.

Force reconstruction is of practical importance to the safety and reliability of plant operations. However, this remains an open problem, and thus far, no universally accepted standard analytical procedure has been available in the public domain. The proposed method can be extended to other mechanical or structural systems that require force estimation. To the best of our knowledge, the application of PINN for load reconstruction presented here is the first of its kind to date. This study also demonstrates the effectiveness of machine learning in engineering applications.

Declarations:

Funding Information: This study did not receive any external funding.

Conflicts of Interest: The authors declare no conflict of interest.

Author contribution: Not Applicable

Data Availability Statement: Not Applicable

Research Involving humans and / or animals: Not Applicable

Informed Consent: Not Applicable

Appendix A

In this section, we state the theorem for the existence of the forward problem (Equations (1 -5)). The function space $H^k(\Omega)$ is a Sobolev Space of order k [26, 29], where k is an integer greater than zero. $H_0^1(\Omega)$ is defined as $\{u(x): u(x) \in H^1(\Omega), u(0) = u(L) = 0\}$

Theorem A1. For $f_k(t) \in C^1[0, T]$, with $k = 1$ to P , the beam equation (Equation (1)) along with BC's Equations (3,4) and IC's Equation (5) has a unique solution (classical sense) $u(t, x)$ with the following regularity:

$$u \in C([0, T]; V) \cap C^1([0, T]; H)$$

Proof. We will start by defining the following function spaces.

$$H = L^2(\Omega)$$

$$V = \{u \in H^3(\Omega) \cap H_0^1(\Omega): D^2u(t, 0) = D^2u(t, L) = 0\}$$

As $\delta(x-x_k) \in H^{-1}(\Omega)$, $D^4u(x, t) \in H^{-1}(\Omega)$ for any fixed t for compatibility.

Equation (14) shows that the eigenvector is bounded (that is $\max. |\phi_n(x)| = \sqrt{\frac{2}{mL}}$).

From Equations (7), (8), and (11), the displacement of the forcing function f_k is.

$$u^k(t, x) = \sum_{n=1}^{\infty} \phi_n(x) \left(\frac{1}{\omega_{dn}}\right) \int_0^t \phi_n(x_k) f_k(\tau) e^{-\zeta_n \omega_n(t-\tau)} \sin(\omega_{dn}(t-\tau)) d\tau$$

.....(A1)

From the superposition principle, the total displacement is

$$u(t, x) = \sum_{k=1}^P u^k(t, x)$$

.....(A2)

We define the term $S_n(t, \tau)$ as representing the integral

$$S_n(t, \tau) = \int e^{-\zeta_n \omega_n(t-\tau)} \sin(\omega_{dn}(t-\tau)) d\tau$$

Integration by parts yields the following

$$S_n(t, \tau) = (1/\omega_n) e^{-\zeta_n \omega_n(t-\tau)} (-\zeta_n \sin(\omega_{dn}(t-\tau)) - \sqrt{1-\zeta_n^2} \cos(\omega_{dn}(t-\tau)))$$

Defining g_n as

$$g_n(t, \tau) = e^{-\zeta_n \omega_n(t-\tau)} (-\zeta_n \sin(\omega_{dn}(t-\tau)) - \sqrt{1-\zeta_n^2} \cos(\omega_{dn}(t-\tau))) \dots \dots \dots (A3)$$

$$S_n(t, \tau) = g_n(t, \tau) / \omega_n \dots \dots \dots (A4)$$

Let us denote the term $T_n^k(t, x) = (\frac{1}{\omega_{dn}}) \int_0^t \phi_n(x_k) f_k(\tau) e^{-\zeta_n \omega_n(t-\tau)} \sin(\omega_{dn}(t-\tau)) d\tau$

Integrating by parts we have

$$T_n^k(t) = (\frac{1}{\omega_{dn}}) (F_n^k(t) S_n(t) - F_n^k(0) S_n(t, 0) - \int_0^t \dot{F}_n^k(\tau) S_n(t, \tau) d\tau) = (\frac{1}{\omega_{dn}}) (\frac{1}{\omega_n}) (F_n^k(t) g_n(t) - F_n^k(0) g_n(t, 0) - \int_0^t \dot{F}_n^k(\tau) g_n(t, \tau) d\tau) \dots \dots \dots (A5)$$

Let $b_n(t) = F_n^k(t) g_n(t) - F_n^k(0) g_n(t, 0) - \int_0^t \dot{F}_n^k(\tau) g_n(t, \tau) d\tau$

As $f_k \in C^1[0, T]$, F_n^k, \dot{F}_n^k are bounded and with (A3) $b_n(t)$ is bounded.

For some positive constants $C_k, C_{k2}, C_{k3}, C_{k4}$ and C_{k5} only dependent of T .

$$|T_n^k(t)| \leq C_{k2} (\frac{|b_n(t)|}{n^4}) \dots \dots \dots (A6)$$

$$|u^k(t, x)| \leq C_k \sum_{n=1}^{\infty} \phi_n(x) (\frac{|b_n(t)|}{n^4})$$

From the convergence of the series $\sum_{n=1}^{\infty} (1/n^4)$

$u^k(t, x) = \sum_{n=1}^{\infty} \phi_n(x) T_n^k(t)$ converges at any arbitrary point (x, t)

$$D^3(u^k(x, t)) \leq C_{k2} \sum_{n=1}^{\infty} \phi_n(x) (\frac{|b_n(t)|}{n}) \leq C_{k3} \sum_{n=1}^{\infty} \phi_n(x) / n$$

Using Parseval's Theorem [37] we have

$$\|D^3(u^k(t, x))\|_{0, \Omega} \leq C_{k4}$$

This implies $u^k(t, x) \in V$ for any $t \in [0, T]$

As $b_n(t) \in C[0, T]$, $\lim_{h \rightarrow 0} u^k(t+h, x) = u^k(t, x)$.

Thus $u \in C([0, T]; V)$.

The modal velocity is,

$$q_n^k(t) = (\frac{1}{\omega_{dn}}) \int_0^t F_n^k(\tau) e^{-\zeta_n \omega_n(t-\tau)} \sin(\omega_{dn}(t-\tau)) d\tau$$

$$\dot{q}_n^k(t) = (\frac{1}{\omega_{dn}}) (\int_0^t F_n^k(\tau) e^{-\zeta_n \omega_n(t-\tau)} (-\zeta_n \omega_n \sin(\omega_{dn}(t-\tau)) + \omega_{dn} \cos(\omega_{dn}(t-\tau))))$$

$$= (1/\sqrt{1-\zeta_n^2}) (\int_0^t F_n^k(\tau) e^{-\zeta_n \omega_n(t-\tau)} (-\zeta_n \sin(\omega_{dn}(t-\tau)) + \sqrt{1-\zeta_n^2} \cos(\omega_{dn}(t-\tau))))$$

Let $I_n(t) = \int_0^t F_n^k(\tau) e^{-\zeta_n \omega_n(t-\tau)} (-\zeta_n \sin(\omega_{dn}(t-\tau)) + \sqrt{1-\zeta_n^2} \cos(\omega_{dn}(t-\tau)))$

Then,

$$\dot{q}_n^k(t) = (1/\sqrt{1 - \zeta_n^2})I_n(t)$$

We define $G_n(t, \tau)$ as

$$G_n(t, \tau) = \int e^{-\zeta_n \omega_n(t-\tau)} \cos(\omega_{dn}(t - \tau)) d\tau$$

Integrating by parts we have

$$G_n(t, \tau) = (1/\omega_n)e^{-\zeta_n \omega_n(t-\tau)}(-\zeta_n \sin(\omega_{dn}(t - \tau)) + \sqrt{1 - \zeta_n^2} \cos(\omega_{dn}(t - \tau)))$$

Hence,

$$G_n = O(1/n^2)$$

.....(A7)

We define h_n as

$$h_n(t, \tau) = -\zeta_n S_n(t, \tau) + \sqrt{1 - \zeta_n^2} G_n(t - \tau)$$

From (A4), (A7) we obtain

$$h_n = O(\frac{1}{n^2})$$

.....(A8)

Integrating by parts we have

$$I_n = F_n^k(t)h_n(t) - F_n^k(0)h_n(t, 0) - \int_0^t \dot{F}_n^k(\tau)h_n(t, \tau)d\tau$$

$$\Rightarrow I_n = O(\frac{1}{n^2})$$

.....(A9)

Hence, $\dot{q}_n(t) = O(\frac{1}{n^2})$ which implies

$$\dot{u}^k(t, x) \leq C_5 \sum_{n=1}^{\infty} \phi_n(x) (\frac{1}{n^2})$$

.....(A10)

Again, from Parseval's Theorem and the convergence of the series $\sum_{n=1}^{\infty} \frac{1}{n^2}$ we have

$$\|\dot{u}^k(t, x)\|_{0,\Omega} \in H$$

Thus $\dot{u}(t, x) = \sum_{k=1}^p \dot{u}^k(t, x)$ is convergent in $C([0, T]; H)$ or,

$u(t, x) \in C^1([0, T], H)$ which implies

$$u \in C([0, T]; V) \cap C^1([0, T]; H) \quad \square$$

Appendix B

This section presents the theorems for the existence and uniqueness of the inverse problem (Equation 16) and their proofs are presented in this section. The standard theorems for the existence and uniqueness of the Volterra Integral Equation (VIE) [30,31] are stated without proofs that are available in the references mentioned in the relevant sections. The main results (existence and uniqueness) for IP are provided in Propositions B4–B6. We assumed that the observational data were consistent (i.e., zero at time $t = 0$).

Theorem B1. The Volterra Integral Equation of the second kind [30]

$$\Phi(t) + \int_0^t K(t, s)\Phi(s)ds = g(t) \quad \text{for} \quad t \in I = [0, T]$$

.....(B1)

with a continuous kernel $K(t, s)$ for each RHS $g(t) \in C[0, T]$, $g(0)=0$ has a unique solution $\Phi(t) \in C[0, T]$.

Proof: See [30,31] for the proof. \square

We now consider the Volterra Integral Equation of the first type [38,39], defined as

$$\int_0^t K(t, s)\Phi(s)ds = g(t) \quad \text{with} \quad t \in I = [0, T]$$

..... (B2)

Theorem B2. With the following assumptions,

- (i) $K(t, s)$ and $\frac{\partial K(t,s)}{\partial t}$ are continuous in $0 \leq s \leq t \leq T$
- (ii) $K(t, t) \neq 0$ for $0 \leq t \leq T$
- (iii) $g(0) = 0$
- (iv) $g(t)$ and $\dot{g}(t)$ are continuous in I

the VIE Equation (B2) has a unique continuous solution.

Proof: See [41] for the proof. □

The rationale behind the above proof is that VIE (B2) can be transformed into VIE (B1) with conditions on kernel $K(t, s)$ and function $g(t)$ as stated in the above lemma.

The results follow from a direct application of **Theorem B1**.

Lemma B3. If $K(t, t) = 0$ for $0 \leq t \leq T$ and if $K(t, s)$ and $g(t)$ are sufficiently differentiable, then VIE Equation (B2) is equivalent to VIE of the second type.

Proof: Differentiating (B2) w.r.t time we have

$$K(t, t)\Phi(t) + \int_0^t \frac{\partial K(t,s)}{\partial t} \Phi(s)ds = \dot{g}(t)$$

.....(B3)

Further differentiating (B2) and applying the condition, $K(t, t) = 0$ and we get

$$\frac{\partial K}{\partial t}(t, t)\Phi(t) + \int_0^t \frac{\partial^2 K(t,s)}{\partial t^2} \Phi(s)ds = \ddot{g}(t)$$

.....(B4)

We define $H(t, s) = \frac{\partial^2 K(t,s)}{\partial t^2} / \frac{\partial K}{\partial t}(t, t)$. Now Equation (B4) is transformed as

$$\Phi(t) + \int_0^t H(t, s) \Phi(s)ds = \ddot{g}(t)$$

.....(B5)

From **Theorem B1**, VIE (B5) has a unique and continuous solution, $\Phi(t)$. □

We now consider the case of a single forcing function f_k acting at point x_k and the observation as the vibration displacements \bar{u}_i at the interior point x_i . We then generalize it to P P-forcing functions.

Proposition B4. Let the system described by Equations (1) to (5) consist of loading at a single point x_k , ($k = K = 1$) with the forcing function f_k which is unknown. Then, f_k can be uniquely determined by solving the inverse problem in Equation (13) with observations at any single interior point. The observations can be the time-history data of the displacement, velocity, or acceleration. To observe the displacement time history, we assumed $f_k \in C^2[0, T]$.

Proof: Number of observation points $M = 1$. We denote the location for the measurements as x_1 and the observed displacement as $u_1(t)$. The force is assumed to act at point x_k . From Equation (16), with $P = 1$, we obtain

$$\bar{u}_i(t) = \sum_{n=1}^N \phi_n(x_1) \left(\frac{\phi_n(x_k)}{\omega_{dn}} \right) \int_0^t f_k(\tau) e^{-\zeta_n \omega_n(t-\tau)} \sin(\omega_{dn}(t-\tau)) d\tau \dots\dots\dots(B6)$$

The above Equation (B6) is a VIE of the first kind.

$$\bar{u}_i(t) = \int_0^t f_k(\tau) K_i^k(t-\tau) d\tau \dots\dots\dots(B7)$$

where $K_i^k(t-\tau) = \sum_{n=1}^{\infty} \phi_n(x_1) \left(\frac{\phi_n(x_k)}{\omega_{dn}} \right) e^{-\zeta_n \omega_n(t-\tau)} \sin(\omega_{dn}(t-\tau))$

By virtue of **Lemma B3**, the VIE (B7) can be transformed into

$$f_k(t) + \int_0^t H_i^k(t,s) f_k(s) ds = \ddot{u}_i(t) \dots\dots\dots(B8)$$

where $H_i^k(t,s) = \frac{\partial^2 K_i^k(t,s)}{\partial t^2} / \frac{\partial K_i^k}{\partial t}(t,t)$

We note that $K_i^k(t,t) = 0$ and $\frac{\partial K_i^k}{\partial t}(t,t) \neq 0$. Now applying **Theorem B3** we can conclude that f_k is a unique and continuous solution to (B6). □

For a system, VIE is expressed in a matrix form as follows

$$\mathbf{f}(t) = \mathbf{g}(t) + \int_0^t \mathbf{K}(t,s) \mathbf{f}(s) ds \dots\dots\dots(B9)$$

Bold letters represent vectors or matrices, and N is the number of elements.

$$\mathbf{f}^T = \{f_1 \ f_2 \ \dots \dots \dots f_N\}^T$$

$$\mathbf{g}^T = \{g_1 \ g_2 \ \dots \dots \dots g_N\}^T$$

$$\mathbf{K} = \{K_{ij}: i = 1 \text{ to } N, j = 1 \text{ to } N\}$$

The following matrix norms will be used for the mathematical proofs.

$$\|\mathbf{f}(t)\| = \max |f_i(t)| \text{ for } i = 1 \text{ to } N \dots\dots\dots(B10)$$

$$\|\mathbf{K}(t)\| = \max \sum_{j=1}^N |K_{ij}|, \ i = 1 \text{ to } N \dots\dots\dots(B11)$$

The existence and uniqueness of the system of integral equation (B9) is shown in the following lemma. This is identical to Theorem 3.11 [30].

Lemma B5. If $\mathbf{g}(t)$ and $\mathbf{K}(t,s)$ are continuous in $0 \leq s \leq t \leq T$ (i.e., all components are continuous), then system (B9) has a unique continuous solution for $0 \leq t \leq T$.

Proof: The proof follows from **Theorem B1**. Only the matrix norms (B10) and B(11) should be used instead of absolute values. □

We define $K_n(t,\tau) = e^{-\zeta \omega_n(t-\tau)} \sin(\omega_{dn}(t-\tau))$. Then the displacement (Equation 13) has the form

$$\bar{u}_i(t) = \sum_{k=1}^P \sum_{n=1}^{\infty} \phi_n(x_i) (1/\omega_{dn}) \phi_n(x_k) \int_0^t f_k(\tau) K_n(t, \tau) d\tau$$

.....(B12)

Defining $\theta_k(t) = \int_0^t f_k(\tau) d\tau$ and $\beta_k(t) = \int_0^t \theta_k(\tau) d\tau$ and integrating by parts Equation (B9) is transformed as

$$\bar{u}_i(t) = \sum_{k=1}^P \sum_{n=1}^{\infty} \phi_n(x_i) (1/\omega_{dn}) \phi_n(x_k) (-\int_0^t \theta_k(\tau) \dot{K}_n(t, \tau) d\tau)$$

.....(B13)

We note that $K_n(t, t) = 0$ and $\theta_k(0) = 0$

We define $\beta_k(t) = \int_0^t \theta_k(\tau) d\tau$

Carrying out similar operation on Equation (B13) we get the following expression

$$\bar{u}_i(t) = \sum_{k=1}^P \sum_{n=1}^{\infty} \phi_n(x_i) (1/\omega_{dn}) \phi_n(x_k) (-\beta_k(t) \dot{K}_n(t, t) + \int_0^t \beta_k(\tau) \dot{K}_n(t, \tau) d\tau)$$

.....(B14)

We note that $\dot{K}_n(t, t) \neq 0$ so VIE (B14) is uniquely solvable.

We now define the following terms

$$\Psi_{ik}(t) = -\sum_{n=1}^{\infty} (\phi_n(x_i) \phi_n(x_k) / \omega_{dn}) \dot{K}_n(t, t)$$

$$\eta_{ik}(t) = \sum_{n=1}^{\infty} (\phi_n(x_i) \phi_n(x_k) / \omega_{dn}) \dot{K}_n(t, t)$$

We now define the following quantities

$$\mathbf{U} = \{u_1 \ u_2 \ \dots \ u_i \ \dots \ u_M\}^T$$

$$\mathbf{H} = \{\beta_1 \ \beta_2 \ \dots \ \beta_i \ \dots \ \beta_P\}^T$$

\mathbf{A} = Matrix of size $(M \times P)$ with an element $A_{ik} = \Psi_{ik}$

\mathbf{B} = Matrix of size $(M \times P)$ with an element $H_{ik} = \eta_{ik}$

$\mathbf{C} = \mathbf{A}^T \mathbf{A}$ Matrix of size $P \times P$

$\mathbf{D} = \mathbf{A}^T \mathbf{B}$ Matrix of size $P \times M$

$\mathbf{V} = \mathbf{A}^T \mathbf{U}$ Vector of size M

With the above terms Equation (B14) can be written in a matrix form

$$\mathbf{U}(t) = \mathbf{A}\mathbf{H}(t) + \int_0^t \mathbf{B}(t, \tau)\mathbf{H}(\tau) d\tau$$

.....(B15)

$$\Rightarrow \mathbf{A}\mathbf{H}(t) = \mathbf{U}(t) - \int_0^t \mathbf{B}(t, \tau)\mathbf{H}(\tau) d\tau$$

.....(B16)

Multiplying VIE (B15) by \mathbf{A}^T we get

$$\mathbf{C}\mathbf{H}(t) = \mathbf{V}(t) - \int_0^t \mathbf{D}(t, \tau)\mathbf{H}(\tau) d\tau$$

.....(B17)

Proposition B6. Let the system described by Equations (1)–(5) consist of loading at multiple interior points x_k ($k = 1, P$) with forcing functions f_k ($k = 1, P$) being unknowns. Subsequently, the IP for determining unknown forces can be reduced to VIE (B14). The forces can be determined from the solution of the VIE. The necessary and sufficient condition for the existence and uniqueness of the solution is that matrix \mathbf{C} should have full rank.

We assume that $u_i \in C^2[0, T]$ (for $i = 1, M$), and with this regularity $f_k \in C[0, T]$ for $k = 1$ to P .

Proof: The basic idea is to recast VIE (B17) into form (B9), which is applicable to systems. Note that the matrix \mathbf{C} is square and of size P (i.e., $M = P$). If it has full rank, it is invertible [32] and VIE (B17) is transformed to

$$\mathbf{H}(t) = \mathbf{C}^{-1}\mathbf{V}(t) - \int_0^t \mathbf{C}^{-1}\mathbf{B}\mathbf{H}(\tau)d\tau \dots\dots\dots(\text{B18})$$

Invoking **Lemma B5**, VIE (B18) has a unique continuous solution $\mathbf{H}(t)$.

The *RHS* of (B18) is continuous. Hence, it follows that if $\mathbf{H}(t)$ is continuous, which implies that $f_k \in C[0, T]$ for $k = 1$ to P . □

References

- 1 Saha, S. Physics Informed Neural Networks (PINN) for the Load Reconstruction for vibrating pipes in Process Plants. In Proceedings of International Conference on Security, Surveillance and Artificial Intelligence (ICSSAI-2023), Kolkata, India, December 1-2, 2023.
- 2 Wachel, J. C.; Morton, S. J.; Atkins, K. E. Piping Vibration Analysis. In Proceedings of Nineteenth Turbo-Machinery Symposium. Houston, Texas, USA, October 1-4, 1990.
- 3 Wachel, J. C. Piping Vibration and Stress. In Proceedings of Machinery Vibration Monitoring & Analysis. Vibration Institute, New Orleans, USA, April 7-9, 1981.
- 4 Coulona, A.; Salanona, R.; Ancian, L. Innovative numerical fatigue methodology for piping systems: qualifying Acoustic Induced Vibration in the Oil&Gas industry. In Proceedings of 7th International Conference on Fatigue Design, Fatigue Design. Senlis, France, November 29-30, 2017. Available online: <https://doi.org/10.1016/j.proeng.2018.02.072>
- 5 Saha, S. Estimation of Point Vibration Loads from Field Measurements for Industrial Piping. *J. Pressure Vessel Technology, Trans. ASME*. **2009**, *131*, 031206. Available online: <https://doi.org/10.1115/1.3109986>
- 6 Saha, S. A Technique for Evaluation of Dynamic Stresses from field Measurements for Vibrating Piping. Recent Patents on Mechanical Engineering 2013, 6.1, 75-82. doi: [10.2174/2212797611206010007](https://doi.org/10.2174/2212797611206010007)
- 7 Peng, L. C.; Peng, A.; Pipe Stress Engineering, 1st ed.; ASME Press; New York, **2009**; pp. 373-457.
- 8 Zeng, L, Jansson, LG, & Börjesson, A. Piping Vibration and Vibration Damage Prevention Through Screening of Dynamic Susceptibility. Proceedings of the 2017 25th International Conference on Nuclear Engineering. Volume 2: Plant Systems, Structures, Components and Materials, ASME, Shanghai, China. July 2–6, 2017. Available online: <https://doi.org/10.1115/ICONE25-66658>
- 9 Motriuk, R. W. Correlation Between Dynamic Strain-Stress and Vibration Based on Field Data. In Proceedings of Pressure Vessels and Piping Conference. Volume, 4: Fluid Structure Interaction ASME, Denver, Colorado, USA, July 17-21, 2005, pp 601-608. Available online: <https://doi.org/10.1115/PVP2005-71536>
- 10 Friswell, M, I.; Mottershead, J. E.; *Finite Element Model Updating in Structural Dynamics*, 1st ed.; Springer Science+Business Media; Dordrecht, Netherlands; 1996; pp. 36-55.
- 11 Kirsch, A.; An Introduction to the Mathematical Theory of Inverse Problems, 2nd ed.; Springer Science+Business Media; New York, USA, 2011; pp. 1-20.
- 12 Isakov V.; *An Inverse Problems for Partial Differential Equations*, 2nd ed.; Applied Mathematical Sciences Vol. 127; Springer, New York, USA, 2006; pp. 1-35.

13. Groetsch, W.; *Inverse Problems in Mathematical Sciences*. 1st ed.; Vieweg + Teubner Verlag; Wiesbaden, Germany; 1993; pp. 5-39 + 67-83.
14. Ang, D.D.; Gorenflo, R.; Le, K. V.; Trong, D. D.; *Moment Theory and Some Inverse Problems in Heat Conduction*, 1st ed.; Springer Verlag; Berlin, Germany; 2002; pp. 1-18.
15. Moussa, W. A; Abdel Hamid, A.N. On the Evaluation of Dynamic Stresses in Pipelines Using Limited Vibration Measurements and FEA in the Time Domain. *Journal of Pressure Vessel Technology, ASME* **1999**, *121*, 37-41. Available online: <https://doi.org/10.1115/1.3109986>
16. Bathe, K. J.; *Finite Element Procedures in Engineering Analysis*. 1st ed.; Prentice-Hall Inc.; Englewood Cliffs, New Jersey, USA, 1982; pp. 114-177 + 235-251 + 499-544.
17. Bruckner, G.; Yamamoto, M. Determination of point wave sources by pointwise observations: stability and reconstruction. *Inverse Problems* **2000**, *16*, 723-748. Available online: doi: [10.1088/0266-5611/16/3/312](https://doi.org/10.1088/0266-5611/16/3/312)
18. Yamamoto, M. Determination of forces in vibrations of beams and plates by point wise and line observations. *J. Inv. Ill-Posed Problems*. **1996**, *4*(5),437-457. Available online: <https://doi.org/10.1515/jiip.1996.4.5.437>
19. Nicaise, S.; Zair, O. Determination of Point Sources in Vibrating Beams by Boundary Measurements: Identifiability, Stability and Reconstruction Results. *Electron. J. Differ. Equations* **2004**,*20*,1–17. Available online: <http://eudml.org/doc/123944>
20. Lagaris, I. E.; Likas, A. Artificial neural networks for solving ordinary and partial differential equations. *IEEE Transactions on Neural Networks* **1998**, *9*(5), 987-1000. Available online: <https://doi.org/10.1109/72.712178>
21. Raissi, M.; Perdikaris, P.; Karniadakis, G. E. Physics-informed neural networks: A deep learning framework for solving forward and inverse problems involving nonlinear partial differential equations. *Journal of Computational Physics* **2019**, *378*, 686-707. Available online: <https://doi.org/10.1016/j.jcp.2018.10.045>
22. Hornik, K.; Stinchcombe, M.; White, H. Multilayer Feedforward Networks are Universal Approximators. *Neural Networks* **1989**, *2*, 359-366. Available online: [https://doi.org/10.1016/0893-6080\(89\)90020-8](https://doi.org/10.1016/0893-6080(89)90020-8)
23. Shin, Y.; Darbon, J.; Karniadakis, E. M. On the Convergence of Physics Informed Neural Networks for Linear Second-Order Elliptic and Parabolic Type PDEs. *Communications in Computational Physics* **2020**, *28*, 2042-2074. Available online: <https://doi.org/10.4208/cicp.OA-2020-0193>
24. Lu, L.; Jin, P.; Pang, G.; Zhang, Z.; Karniadakis, G. E. Learning nonlinear operators via DeepONet based on the universal approximation theorem of operators. *Nature Machine Intelligence* **2021**,*3*(3), 218-229. Available online: <https://doi.org/10.1038/s42256-021-00302-5>
25. Clough, R. W.; Penzien, J.; *Dynamics of Structures*, 3rd ed.; Computers & Structures Inc.; New York, USA; 2003; pp. 87-91+169-179+365-373.
26. Oden, J. T.; Reddy, J. N.; *An Introduction to the Mathematical Theory of Finite Elements*, 1st ed.; Dover Publications Inc.; New York, USA, 2011; pp. 9-31+55-56+108-112.
27. Wang, S.; Yu, J.; Perdikaris, P. When and why PINNs fail to train: A neural tangent kernel perspective. *Journal of Computational Physics*, **2021**, *449*, 110768. Available online: <https://doi.org/10.1016/j.jcp.2021.110768>

28. Jacot, A.; Gabriel, F.; Hongler, C. Neural tangent kernel: Convergence and generalization in neural networks. *Advances in neural information processing systems* **2018**, 8571–8580. Available online: <https://doi.org/10.48550/arXiv.1806.07572>
29. Curtain, R. F.; Pritchard, A. J.; *Functional Analysis in Modern Applied Mathematics*, 1st ed.; Academic Press; New York, USA, 1977; pp. 55-74.
30. Linz, P., *Analytical and Numerical Methods for Volterra Equations*, 1st ed.; SIAM: PA, USA, 1985; pp. 29-37.
31. Kress, R., *Linear Integral Equations*, 1st ed.; Springer Verlag: New York, USA, 1989; pp. 33-34.
32. Blythe, T. S; Robertson, E. F., *Basic Linear Algebra*, 2nd ed.; Springer Verlag; London, Great Britain, 2002, pp. 37-65.